SUPPLEMENTARY DATA

Enrichment of human prostate cancer cells with tumor initiating properties in mouse and zebrafish xenografts by differential adhesion

Nitu Bansal, Stephani Davis, Irina Tereshchenko, Tulin Budak-Alpdogan, Hua Zhong, Mark N. Stein, Isaac Yi Kim, Robert S. DiPaola, Joseph R. Bertino, Hatem E. Sabaawy

SUPPLEMENTARY METHODS

Cell Culture, prostate spheres, colony formation, migration, and invasion assays

Prostate cancer cells Du145, PC3, CWR22 and LnCap cells were generated from stocks maintained at CINJ, and were originally purchased from ATCC. Cells were cultured at low passage numbers in RPMI media (GIBCO) supplemented with 10% fetal bovine serum (FBS), and 1% penicillin-streptomycin. For all the attachment experiments, early passage cells were used. For colony forming and clonogenic assays, 200 prostate cancer cells were plated in 6-well plates. After 2 weeks, the plates were washed in 1x PBS, and cells were stained with crystal violet. Colonies of >50 cells were counted. Prostate spheres were generated in 1% agarose in keratinocyte serum free media (KSFM) media. The spheroids grown on 1% agarose were cultured in KSFM supplemented with epidermal growth factor (EGF), basic fibroblast growth factor (bFGF), and bovine pituitary extract (All from Invitrogen) (1). Collagen-I-adherent cells at 5 minutes, and non-adherent cells after 20 minutes were suspended at 2 x 10^3 cells/well in KSFM media. Every 3 days, half of the media was replaced, and spheres consisting of >50 cells were counted on day14. Single cells from day-7 spheroids were used in secondary spheroid assays. RWPE (normal prostate cells) were also cultured in KSFM as recommended by ATCC.

In migration assays, cells were plated in 0.5% FBS media in transwell chambers with the lower chambers contained growth media with 10% FBS. After 48 hrs, cells that migrated to the lower surface of transwell inserts were stained with crystal violet and counted. In invasion assays, cells were plated on matrigel-coated transwell inserts and assayed.

Primary prostate cancer tissue dissociation and culture of primary cells

Human primary prostate cancer tissues were obtained by radical prostatectomy (IRB approved). For isolation of single cells, the tissue was minced into smaller pieces and incubated for 2-4 hrs at 37ºC in RPMI media supplemented with 10% FBS, 1% Anti-anti (Invitrogen), 200U/ml collagenase I (Sigma Aldrich, USA), 0.5mg/ml Dispase II (Stem Cell

Technologies). After 4 hrs, the digested tissue pieces were filtered through 100 μm cell strainers (BD Falcon), and centrifuged at 250g for 30 seconds. Cell pellets were then washed once with 1xPBS and centrifuged once more at 250g for 30 seconds. The final cell pellet was suspended in prosta life media (Lifeline Technologies) and plated in T25 flasks. The media was changed once every 3 days.

Flow cytometry and cytotoxicity assays

Cells obtained after attachment assay or after treatments were collected and washed twice in 1xPBS. 1x 10^6 cells were then suspended in 1xPBS and stained with the antibodies conjugated with either FITC or PE and APC. After 30 mins of incubation in dark, cells were washed with PBS and suspended in 5μl of 7AAD. The cells were then acquired using FACS Calibur instrument. Both acquisition and analysis were done using Cell Quest software. Antibodies used for flow were CD49b (β1-Integrin)-FITC (Millipore), CD44-APC, CD133-PE and 7-AAD (purchased from DB Biosciences).

Cytotoxicity of methotrexate and other chemotherapies were assayed following a 3-day exposure. Prostate cancer cells (3 x 10^3 cells/well) were treated with multiple concentrations to determine an IC_{50}, cell growth was monitored over time and resulting cytotoxicity was analyzed using MTS assay (Sigma) per manufacturer's instructions.

IHC for validation of prostate cancer epithelium and chromosomal rearrangements

Each prostate cancer sample was subjected at diagnosis to histological examination of the H&E slides to determine tumor regions, and consecutively cut slides from these core regions were utilized for IHC and interphase FISH. For IHC, formalin fixed paraffin-embedded (FFPE) tissue samples from biopsies and xenografts were stained with selected antibodies using antigen retrieval, and sections were scored for percentage of cells and intensity on a 0-2 scale by pathologists blinded to cell fractions. First, the H&E slide and α-methylacyl-coenzyme-A racemase (AMACR)-immunostained sections were reviewed by qualified pathologists. Overexpression of AMACR in prostate cancer cells was detected by IHC using a monoclonal rabbit anti-human P504S antibody (clone 13H4, Cell Marque). After tumor regions were determined, consecutive slides were included in FISH analysis. Overexpression of ERG gene in prostate cancer cells that were harboring TMPRSS2-Erg fusion was detected by IHC using a monoclonal rabbit anti-human ERG antibody (clone EP111, Dako).

Interphase FISH validation of rearrangements

ERG gene rearrangement was assessed using a newly developed break-apart interphase FISH assay optimized from a previously described protocol (2) with modifications. In brief, the TMPRSS2-Erg rearrangement probes were optimized to detect the deletion between TMPRSS2 and ERG at 21q22 associated with the TMPRSS2-Erg fusion in a triple-color deletion assay. Optimization included the incorporation of additional bacterial artificial chromosome (BAC) probes for the detection of gene fusions (Irina Tereshchenko and Robert S. DiPaola; unpublished data). All BACs were obtained from the BACPAC Resource Center (Oakland, CA, USA). DNA probes were synthesized using 5-(3-aminoallyl)-dUTP-nick translation and the ARES Alexa Fluor DNA Labeling Kit (Molecular Probes, Invitrogen, USA). For detection of ERG rearrangements and TMPRSS2-ERG fusion, we used the following probes: RP11-95I21 (Alexa Fluor 555-labeled; 5' to ERG), RP11-476D17 (Alexa Fluor 488-labeled; 3' to ERG), and RP11-35C4 (Alexa Fluor 647-labeled; 5' to TMPRSS2). Labeled samples on FISH slides were scanned using a confocal microscope (Zeiss LSM 510 META, 100x objective). Image stacks of 300 nm z-step size were captured and analyzed using Imaris Software (Bitplane). At least 50-100 nuclei were evaluated per tissue section, whenever it was possible.

Extreme Limiting dilution analysis (ELDA)

To assess the number of self-renewing cells contained within the bulk of the primary prostate cancer mass, QD-labeled primary prostate cancer cells were propagated and 5 min collagen-attached $\alpha 2\beta 1^{hi}$/$CD44^{hi}$ cells were isolated, and introduced SC into 48 hpf zebrafish recipients at limiting dilution (1×10^3, 1×10^2, 1×10^1, and 3 cells/embryo), with purity of 98-99%, and viability 95-99.9% (n=50 embryos injected/tumor case). Engraftment was assessed starting at 5 days post transplantation by fluorescence microscopy. Embryos that showed engraftment at day 5 and latter on died from disseminated tumors were scored positive for tumor initiation. The TIC frequency was finally calculated after 12 dpt using linear regression method completed using ELDA at http://bioinf.wehi.edu.au/cgi-bin/limdil/limdil.pl. ELDA have the capacity to calculate frequencies for stem cell subpopulations that produce 0% or 100% tumor engraftment, and therefore is preferred for calculating tumor initiation from limited cell numbers. Accuracy of this test is determined by correlation coefficient (R^2 values), and provided 99% confidence intervals to compare tumor-initiating cell numbers between samples. To verify these data, we have also used L-Calc statistical software (Stem cell technologies) for limiting dilution analysis

(LDA), and subsequent analyses provided 95% confidence intervals and *t* test statistical values that distinguished between the numbers of TIC from the three fractions of cells investigated.

SUPPLEMENTARY REFERENCES

1. Mimeault M, Johansson SL, Batra SK. Pathobiological implications of the expression of EGFR, pAkt, NF-kappaB and MIC-1 in prostate cancer stem cells and their progenies. PLoS One 2012;7:e31919.

2. Mehra R, Tomlins SA, Shen R, et al. Comprehensive assessment of TMPRSS2 and ETS family gene aberrations in clinically localized prostate cancer. Mod Pathol 2007;20:538-44.

SUPPLEMENTARY FIGURE LEGEND

Supplementary Fig 1. Morphology and proliferation of different collagen adherent fractions. **A**: Cell proliferation of the subfractions of collagen adherent cells during culture for 6 days. **B:** Light phase microscopic images of DU145 and PC3 cells after 1 and 6 days of culture. Images are taken at 10X magnification. DU145 cells were most confluent at imaging. Scale bar is 100 μM in all DU145 and PC3 image panels.

Supplementary Fig. 2. Collagen-adherent cells are enriched in putative TICs. **A:** Mean percentage of 5` adherent and 20` non-adherent fractions of cells with $\alpha2\beta1^{hi}/CD44^{hi}$ phenotype in PC3, PC3 spheroids, CWR22, and CWR22 spheroids. Data represent three independent experiments performed in triplicates. **B:** Flow cytometric analyses of CWR22 and LnCap cells after collagen adherence showing higher mean fluorescence intensity (MFI) of 5 minutes collagen-I-adherent ($\alpha2\beta1^{hi}/CD44^{hi}$) cells (Adherent) compared to 20 min-non-adherent ($\alpha2\beta1^{low}/CD44^{low}$) cells (Non-adherent), and IgG control (IgG). **C:** CD133 expression in various subsets of CWR22 cells. In a representative experiment, 0.1% of the cells were $\alpha2\beta1^{hi}/CD44^{hi}$/CD133 positive, and spheroids from these $\alpha2\beta1^{hi}/CD44^{hi}$ cells showed upregulated CD133 expression to 1.42% (*$p<0.001$).

Supplementary Fig. 3. Self-renewal and *in vitro* tumorigenic potential of collagen-adherent $\alpha2\beta1^{hi}/CD44^{hi}$ cells. **A:** Bars demonstrate the enhanced ability of single $\alpha2\beta1^{hi}/CD44^{hi}$ cells to form spheroids, compared to the limited ability of single $\alpha2\beta1^{low}/CD44^{low}$ cells. **B:** Images from $\alpha2\beta1^{low}/CD44^{low}$-derived spheroids that stopped growing at day 9. Scale bars are 50 μm. **C:** Quantitation of secondary spheroids from $\alpha2\beta1^{hi}/CD44^{hi}$ and $\alpha2\beta1^{low}/CD44^{low}$ single cells derived from primary spheroids at day-7. Numbers of spheroids are displayed as mean ± s.e.m, and were done in triplicate. **D:** IC_{50} concentrations of various drugs used. IC_{50}s were determined using MTS assays in DU145 cells. **E:** DU145 cells were treated with the clinically used chemotherapy drugs at IC_{50} concentrations. Collagen-adherent cells at 5-minutes were measured using MTS assays. Values are represented as mean fold of 5 minute-adhesion ± S.D. from three independent experiments. There was a lack of significant inhibition of 5 min-adhesion in cells treated with taxotere and cisplatinum (# $p>0.05$), a non-significant increase in adhesion with doxorubicin (^ $p>0.05$), and a statistically significant increase in adhesion with methotrexate and carboplatinum (* $p<0.05$) suggesting resistance.

Supplementary Fig 4. Diagnostic images of prostate cancers based on histological H&E examination. **A-F:** Formalin fixed paraffin embedded (FFPE) sections from two representative primary prostate cancer (PCa) tissues used for generating zebrafish xenografts. Sections of PCa tissues from patient #5 (**A-C**) and patient #6 (**D-F**) were stained with H&E, and imaged. The H&E images in **B-C** and **E-F** are higher magnifications of the outlined areas in **A** and **D**, respectively. Inset in **F** is a 500X magnification of the outlined area in the same panel. An H&E image in the main figures (Fig. 5J) represents a 500X magnification of the outlined area (*) in this supplementary Fig.4C from same patient's tissue.

Supplementary Fig 5. Expression of Erg and AMACR in primary PCa tissues. FFPE sections from primary PCa tissues were used to detect the overexpression of both Erg, due to the presence of TMPRESS2:Erg fusions, and AMACR proteins in PCa cells by IHC. **A-D:** Two representative cases of PCa cells that are either negative (**A-B**) or positive (**C-D**) for Erg expression in brown. Notice that in both cases, endothelial cells demonstrated a strongly positive Erg expression (arrow), and were used as an internal positive control. The images in **B** and **D** are higher magnifications of the outlined areas in **A** and **C**, respectively. **E-H:** Two representative cases of PCa cells that are positive for AMACR expression. The sections in (**G-H**) are from the same tissues that are positive for Erg expression in (**C-D**), therefore, Erg overexpression correlates with AMACR expression in these PCa cells that harbor the TMPRESS-Erg fusion. AMARC expression either in brown (**E-F**) or in red (**G-H**) was detected as a strong cytoplasmic granular staining. The images in **F** and **H** are higher magnifications of the outlined areas in **E** and **G**, respectively. An AMACR IHC image in the main figures (Fig. 5J) represents a higher magnification of the outlined area (*) in this supplementary Fig.5F from the same patient's tissue. **I-J:** Dual IHC for Erg and AMACR expression in a section from a PCa patient with no known TMPRSS:Erg fusions. The sections in (**I-J**) are from the same tissues that are negative for Erg expression in (**A-B**), therefore, AMACR expression may be used to identify PCa cells that do not express Erg when these PCa cells do not harbor the TMPRESS-Erg fusion. Notice that endothelial cells demonstrated a strongly positive Erg expression (arrow), and were used as an internal positive control.

Supplementary Fig 6. Expression of Erg and AMACR in primary PCa cells harboring the TMPRESS-Erg fusion and were used to generate zebrafish xenografts of primary PCa cells. **A-F:** Control sections from primary PCa tissues known to overexpress Erg, due to the presence of TMPRESS2:Erg fusion. **A:** H&E. **B:** Erg overexpression. **C:** AMACR overexpression. **D-E:** Dual Erg/AMACR expression in PCa cells by IHC. The image in **E** is a higher magnification of the

outlined area in **D**. **F:** Multicolor interphase FISH on cells from the same patient tissues in A-E demonstrating TMPRESS:Erg rearrangements. The translocation is demonstrated through split of red and green signals representing the rearranged ERG allele, while juxtaposition of green and white signals (arrow) designates the TMPRESS:Erg fusion. **G-I:** IHC and interphase FISH sections from primary PCa patient #5, with TICs that were used to generate zebrafish xenografts. The image in **H** is a higher magnification of the outlined areas in **G**. An Erg overexpression IHC image in the main figures (Fig. 5J) represents a 500X magnification of the outlined area (*) in this supplementary Fig.6H from a sequential section of the same #5 patient's tissue. **I:** Multicolor interphase FISH on cells from the same #5 patient's tissues in **G-H** demonstrating TMPRESS:Erg rearrangements. The intact ERG allele is designated by juxtaposition of red and green signals. The TMPRESS:ERG gene fusion was detected through deletion with the absence of a red signal and remaining green signal. Please note that TICs from this same primary PCa patient #5 were used to generate zebrafish xenografts, and cells from these xenografts showed strong nuclear staining for Erg by IHC (Fig. 5J), suggesting that these fish xenografts were derived from primary PCa cells, and not from normal epithelial cells. Scale bars are 2 μm in **F** and **I**.

Supplementary Fig. 7. IHC analyses of xenografts of human prostate cancer cells in embryonic zebrafish. **A-D:** Sections from zebrafish embryo with prostate cancer xenografts migrating to the tail region (**A-D**). Migrated cells are stained with H&E (**A-B**), and CK8-18 (**C-D**). **B-D** are higher magnification of the outlined area in **A**. **D** is a higher magnification of the outlined area in **C**. **E:** Localized xenograft outlined (**E**), and sections were stained with either H&E (**F**), or in dual IHC with the combination of PSA in red and hCD44 in brown (**G-H**). Notice the faint cytoplasmic red staining of PSA (arrows) with the overlying brown stating of hCD44. **F-H** are higher magnification of the outlined area in **E**. **H** is a higher magnification of the outlined area in **G**. Images were taken at 9 dpt for **A-D** and 8 dpf for **E-H**. Scale bars are 100 μm in **A** and **E**.

Supplementary Fig. 8. ELDA plot used to assess the frequency of self-renewing TICs. TIC frequencies were calculated using ELDA with 99% confidence interval. Correlation coefficient (R2) values are displayed. While the TIC potential for $\alpha2\beta1^{low}/CD44^{low}$ cells was limited (green lines), the 99% confidence interval for DU145 parental cells, and for $\alpha2\beta1^{hi}/CD44^{hi}$ cells sorted from 5-min-adherent fraction at correlation coefficient (R2) values of ≥0.99 were 1/175 to 1/338 and 1/75 to 1/125, respectively. This correlates to a frequency of self-renewing TIC of 0.296% to 0.57% in DU145 parental cells, and 0.8% to 1.33% in $\alpha2\beta1^{hi}/CD44^{hi}$ cells sorted from 5-min-adherent fraction. The overall frequency of

self-renewing TICs was calculated to be 0.3% to 1.3% of DU145 cells. These data were further confirmed using the L-calc software as described in supplemental methods. ELDA was used to assess the frequency of self-renewing tumor initiating PC3 and primary cells similarly (Not shown).

Supplementary Fig. 9. Xenotransplant of human prostate cancer cells in conditioned juvenile Casper zebrafish. **A**: Fluorescent image from a control untransplanted Casper zebrafish with background fluorescence within the gut region and in the eye. **B-E**: DU145 parental, 5-min adherent $\alpha2\beta1^{hi}$/$CD44^{hi}$ cells, and 20-min non-adherent $\alpha2\beta1^{low}$/$CD44^{low}$ cells were transplanted either SC in the tail region, or IP into 6-8 weeks Casper zebrafish. Recipient fish were conditioned with dexamethazone for 2 days before transplant. Non-tumor normal prostate cells were used as control and yielded no tumor formation (Supplementary Table 4). **B-C**: Representative fluorescent images from recipient fish transplanted with 5×10^2 parental DU145 cells SC (circled area) with tumor growth (**B**) and localized tumor spread (**C**) in the same fish at 13 and 28 dpt. The three right panels show both histology of the tumor growth in **B** (top), and 40X magnification of the circled area in **C** (middle panel is bright field and lower panel is 605 red fluorescence). **D-E**: A second representative fish from those transplanted with 5×10^1 5-min adherent $\alpha2\beta1^{hi}$/$CD44^{hi}$ sorted cells with tumor spread in the tail region (arrow in **E**) and to the brain (circled area above the eye in **E**). All images are lateral views with the zebrafish head to the left.

Supplementary Fig. 10. Metastatic behavior of prostate cancer cells *in vivo* in zebrafish xenografts. **A-H:** Histological sections stained with H&E from control untransplanted zebrafish muscle (**A-B**) and kidney marrow (**E-F**) tissues compared to matching sections from fish transplanted with the 5-min collagen-attached $\alpha2\beta1^{hi}$/$CD44^{hi}$ cells (**C-D** and **G-H**). Muscle section of control fish in low power (**A**) and high power (**B**) images demonstrates no cell infiltrates, while the corresponding muscle section of control fish in low power (**C**) and high power (**D**) images shows widespread tumor cell infiltrates (white arrow). Notice the round morphology of the DU145 engrafted cells compared to the elongated muscle nuclei. **E-H:** Histological H&E sections from a control non-transplanted juvenile zebrafish kidney marrow in **E**, and in higher power in **F** showing kidney tubules and marrow hematopoietic tissue (white arrow). The section from the DU145 TICs transplanted fish at day-13 post-transplant demonstrates fewer tubular structures, and tumor infiltrates and colonies of cells (black arrows) resembling the morphology of human DU145 tumor cells. **I:** Sections from muscle metastatic dissemination were subjected to IHC with anti-hCD44 demonstrating engrafted human DU145 cells. Data represent sections from recipient fish fixed at day 28 (n= 6/group). Scale bars are 50 μm in **A-H**, and 20 μm in **I**.

Table S1

DU145 Zebrafish Embryonic Transplant	Transplant embryos (Survivors)	Local growth	Dissemination potential (Presence of QD micro-metastasis at 3 dpt) (%)						
			Muscle	Yolk	Brain**	Micro-metastasis			
						<5	5-10	>10	Total [>5] tumor **(%)**
SC Vehicle	10 (9)	0 (0)	0 (0)	0 (0)	0 (0)	0 (0)	0 (0)	0 (0)	0 **(0)**
SC 10 cells									
Parental	50 (36)	4 (11)	19 (53)	18 (50)	12 (33)	2 (14)	10 (34)	15 (42)	25 **(69)**
Non-TICs	50 (38)	5 (13)	7 (18)	8 (21)	5 (13)	5 (14)	3 (61)	5 (14)	8 **(21)**
TICs	50 (40)	4 (10)	25 (62)	22 (55)	20 (40)	2 (40)	5 (40)	27 (40)	32 **(80)***
3 cells									
Parental	50 (42)	3 (7)	10 (24)	11 (26)	10 (24)	1 (42)	4 (42)	7 (42)	11 **(26)**
Non-TICs	50 (36)	0 (0)	6 (17)	5 (14)	2 (6)	2 (36)	2 (36)	4 (36)	6 **(17)**
TICs	50 (45)	3 (7)	20 (44)	20 (40)	17 (38)	2 (45)	2 (45)	20 (45)	22 **(49)***
SC 10 normal cells									
Parental	20 (17)	0 (0)	0 (0)	0 (0)	0 (0)	3 (18)	0 (0)	0 (0)	0 (0)
Non-TICs	20 (15)	0 (0)	0 (0)	0 (0)	0 (0)	2 (13)	0 (0)	0 (0)	0 (0)
Yolk 10 cells									
Parental	50 (44)	10 (23)	5 (11)	10 (23)	5 (11)	5 (44)	6 (44)	11 (44)	17 **(39)**
Non-TICs	50 (45)	15 (33)	1 (2)	2 (4)	0 (0)	3 (45)	2 (45)	2 (45)	4 **(9)**
TICs	50 (40)	13 (32)	8 (20)	14 (35)	6 (15)	3 (40)	8 (40)	14 (40)	22 **(55)***
3 cells									
Parental	50 (38)	5 (13)	3 (8)	7 (18)	3 (8)	4 (38)	4 (38)	7 (38)	11 **(29)**
Non-TICs	50 (42)	7 (17)	2 (5)	4 (10)	0 (0)	1 (42)	0 (42)	4 (42)	4 **(10)**
TICs	50 (42)	2 (5)	10 (24)	16 (38)	4 (10)	1 (42)	6 (42)	16 (42)	22 **(52)***

Table S1. Prostate tumor cell transplantation in embryonic zebrafish demonstrates tumor initiation potential of TICs. Embryos were transplanted in three independent experiments using 20 embryo/variable in two experiments, and 10 embryos/variable in a third experiment. Parental DU145 cells, non-collagen adherent cells at 20-min that were sorted for $\alpha2\beta1^{low}$/$CD44^{low}$ cells (Non-TICs), and 5-min collagen adherent cells that were sorted for $\alpha2\beta1^{hi}$/$CD44^{hi}$ (TICs) were injected either subcutaneously (SC) or into the yolk (Yolk) of 48-hpf zebrafish embryos at the indicated cell doses. Local tumor growth at the yolk resulted in an overall lower potential for tumor dissemination to distant sites compared to SC tumor growth, likely due to differences in nutritional microenvironments. Dissemination potential of injected cells in fish embryos was defined by the presence of migrating quantum dot (QD)-labeled cells at distant sites from the site of injection at 3-days post transplantation (dpt). Micro-metastasis was frequently detected at multiple distant sites simultaneously in the same embryo. The presence of >5 micro-metastasis sites was considered as an evidence for tumor growth and dissemination. Vehicle (PBS)- or QDs only-injected embryos did not develop any tumors. *TICs initiated significantly higher tumors than parental or non-TICs, ANOVA, $p< 0.001$ in all cell doses and injection sites. **Brain metastasis were present significantly higher in embryos injected with the TICs fraction, Fisher's exact test, $p< 0.001$. ***Tumor initiation potential of pretreated cells was significantly lower than untreated cells, n= ≥20, Fisher's exact test, $p< 0.02$.

Table S2

Prostate cancer Zebrafish Embryonic Transplant	**Transplant embryos** (Survivors)	**Dissemination potential** (Presence of QD micro-metastasis at 12 dpt) (%)
PC3 cells		
Adherent $\alpha2\beta1^{low}/CD44^{low}$	23 (18)	11 (61)*
Non-adherent $\alpha2\beta1^{hi}/CD44^{hi}$	22 (17)	6 (35)
Non-adherent $\alpha2\beta1^{low}/CD44^{low}$ (Non-TICs)	20 (18)	2 (11)
DU145 cells		
Adherent $\alpha2\beta1^{low}/CD44^{low}$	25 (19)	10 (53)
Non-adherent $\alpha2\beta1^{hi}/CD44^{hi}$	25 (23)	8 (35)
Non-adherent $\alpha2\beta1^{low}/CD44^{low}$ (Non-TICs)	25 (20)	7 (35)

Table S2. Tumor initiation potential of the different prostate cancer cell fractions from collagen-I adhesion. Embryos were transplanted in two independent experiments using >20 embryos/variable. Collagen-I-adherent cells and collagen-I-non-adherent PC3 and DU145 cells at 20-min were sorted for $\alpha2\beta1^{low}/CD44^{low}$ and $\alpha2\beta1^{hi}/CD44^{hi}$ cells. Sorted cells were injected into 48-hpf zebrafish embryos. The dissemination potential of injected cells into zebrafish embryos was defined by the presence of migrating labeled cells at distant sites from the injection site at 12 days post transplantation (dpt) to allow for testing the full range of tumor initiation. *PC3-adherent $\alpha2\beta1^{low}/CD44^{low}$ tumor initiation potential was significantly higher than non-TICs (Fisher's exact test, two-sided p-value=0.004). All other comparisons were not significantly different.

Table S3

Prostate cancer Zebrafish Embryonic Transplant		Transplant embryos (Survivors)	Dissemination potential (Presence of QD micro-metastasis at 3 dpt) (%)
PC3 cells			
	Parental	45 (37)	25 **(68)**
	Non-TICs	40 (30)	18 **(60)**
	TICs	32 (28)	24 **(86)**[1]
CWR22 cells			
	Parental	25 (18)	10 **(56)**
	Non-TICs	32 (24)	6 **(25)**
	TICs	45 (35)	22 **(63)**[2]
LnCap cells			
	Parental	30 (26)	17 **(65)**
	Non-TICs	20 (16)	10 **(62)**
	TICs	22 (20)	18 **(90)**[3]
Primary #2 cells			
	Parental	25 (18)	11 **(29)**
	Non-TICs	18 (15)	6 **(10)**
	TICs	20 (18)	15 **(52)**[4]
Primary #3 cells			
	Parental	23 (16)	14 **(87)**
	Non-TICs	22 (15)	13 **(87)**
	TICs	22 (19)	18 **(95)**[5]
Primary #6 cells			
	Parental	40 (36)	24 **(67)**
	Non-TICs	33 (25)	10 **(40)**
	TICs	45 (37)	32 **(87)**[6]

Table S3. Multiple prostate cancer cell lines and primary tumor cell transplantation in embryonic fish demonstrates tumor initiation potential of TICs. Embryos were transplanted in two independent experiments using >20 embryo/variable. Parental cells, non-collagen adherent cells at 20-min that were sorted for $\alpha2\beta1^{low}$/$CD44^{low}$ cells (Non-TICs), and 5-min collagen adherent cells that were sorted for $\alpha2\beta1^{hi}$/$CD44^{hi}$ (TICs) were injected SC in 48-hpf zebrafish embryos. The dissemination potential of injected cells in zebrafish embryos was defined by the presence of migrating quantum dot (QD)-labeled cells at distant sites from the site of injection at 3-days post transplantation (dpt). The presence of >5 micro-metastasis sites was considered an evidence for tumor growth and dissemination. Data from prostate cancer cell lines and three representative primary prostate cancer patient samples are demonstrated. [1]PC3-TICs were significantly higher than non-TICs, Fisher's exact test, two-sided p-value=0.04. [2]CWR22-TICs were significantly higher than non-TICs, Fisher's exact test, two-sided p-value=0.007. [3]LnCap-TICs showed a trend to be higher than non-TICs, Fisher's exact test, two-sided p-value=0.1034. [4]Primary-#2-TICs were significantly higher than non-TICs, Fisher's exact test, two-sided p-value=0.014. [5]Primary-#3-TICs were not significantly different from non-TICs, Fisher's exact test, two-sided p-value=0.57. [6]Primary-#6-TICs were significantly higher than non-TICs, Fisher's exact test, two-sided p-value=0.0002.

Table S4

	DU145 Juvenile Zebrafish Xenograft	Transplant zebrafish (Survivors)	Local growth	Dissemination potential (Presence of QD micro-metastasis at 28 dpt) (%)						
				Muscle	Marrow	Brain**	Micro-metastasis			
							<5	5-10	>10	Total [>5] tumor (%)
SC	**500 cells**									
	Parental	3 (3)	1 (33)	2 (67)	2 (67)	2 (67)	0 (0)	0 (0)	2 (67)	2 **(67)**
	Non-TICs	3 (3)	0 (0)	1 (33)	1 (33)	1 (33)	0 (0)	0 (0)	1 (33)	1 **(33)**
	TICs	3 (3)	1 (33)	3 (100)	2 (67)	2 (67)	0 (0)	0 (0)	3 (100)	3 **(100)**
	50 cells									
	Parental	3 (3)	0 (0)	3 (100)	3 (100)	3 (100)	0 (0)	0 (0)	3 (100)	3 **(100)**
	Non-TICs	3 (3)	0 (0)	0 (0)	0 (0)	0 (0)	0 (0)	0 (0)	0 (0)	0 **(0)**
	TICs	3 (3)	1 (33)	3 (100)	3 (100)	3 (100)	0 (0)	0 (0)	2 (67)	3 **(100)**
	10 cells									
	Parental	3 (2)	0 (0)	2 (67)	1 (33)	0 (0)	0 (0)	0 (0)	2 (67)	2 **(67)**
	Non-TICs	3 (3)	0 (0)	1 (33)	1 (33)	1 (33)	0 (0)	0 (0)	1 (33)	1 **(33)**
	TICs	3 (3)	0 (0)	2 (67)	2 (67)	2 (67)	0 (0)	0 (0)	2 (67)	2 **(67)**
IP	**500 cells**									
	Parental	3 (3)	2 (67)	1 (33)	0 (0)	0 (0)	0 (0)	0 (0)	1 (33)	3 **(100)**
	Non-TICs	3 (3)	0 (0)	1 (33)	0 (0)	0 (0)	0 (0)	0 (0)	1 (33)	1 **(33)**
	TICs	3 (3)	1 (33)	3 (100)	2 (67)	2 (67)	0 (0)	1 (33)	1 (33)	2 **(67)**
	50 cells									
	Parental	3 (3)	1 (33)	2 (67)	1 (33)	3 (100)	0 (0)	1 (33)	1 (33)	3 **(100)**
	Non-TICs	3 (3)	0 (0)	0 (0)	0 (0)	0 (0)	0 (0)	0 (0)	0 (0)	0 **(0)**
	TICs	3 (3)	0 (0)	3 (100)	3 (100)	3 (100)	0 (0)	1 (33)	2 (67)	3 **(100)**
	10 cells									
	Parental	3 (3)	0 (0)	2 (67)	1 (33)	0 (0)	0 (0)	1 (33)	0 (0)	1 **(33)**
	Non-TICs	3 (3)	0 (0)	0 (0)	0 (0)	0 (0)	0 (0)	0 (0)	0 (0)	0 **(0)**
	TICs	3 (3)	1 (33)	2 (67)	2 (67)	2 (67)	0 (0)	0 (0)	2 (67)	3 **(100)***

Table S4. Prostate tumor cell transplantation in juvenile conditioned zebrafish demonstrates the metastatic potential of TICs. Juvenile 6-8 week zebrafish were conditioned with 10 μg/ml dexamethazone for 2 days as described [28]. On the next morning, fish were anesthetized with tricaine, and transplanted in three independent experiments using 9 juvenile fish/cell dose. QD-labeled parental DU145 cells, non-collagen adherent cells at 20-min that were sorted for $\alpha2\beta1^{lo}/CD44^{lo}$ cells (Non-TICs), and 5–min collagen adherent cells that were sorted for $\alpha2\beta1^{hi}/CD44^{hi}$ cells (TICs) were injected either SC in the tail region, or IP at the indicated cell doses. The dissemination potential of injected cells in zebrafish was defined by the presence of migrating QD-labeled cells at distant sites from

the site of injection at days 13- and 28-dpt. The presence of >5 micro-metastasis sites was considered as an evidence for tumor growth and metastasis. Dissemination was frequently detected at multiple distant sites including brain, muscle, and kidney marrow with multiple colonies detected simultaneously after local growth in the same recipient zebrafish. Vehicle (PBS)- or QDs only-injected fish did not develop any tumors. *TICs initiated significantly higher tumors than parental or non-TICs, ANOVA, $p < 0.001$ in all doses and injection sites. **Brain metastases were present at a significantly higher rate in fish injected with the TICs fraction, Fisher's exact test; $p < 0.001$.

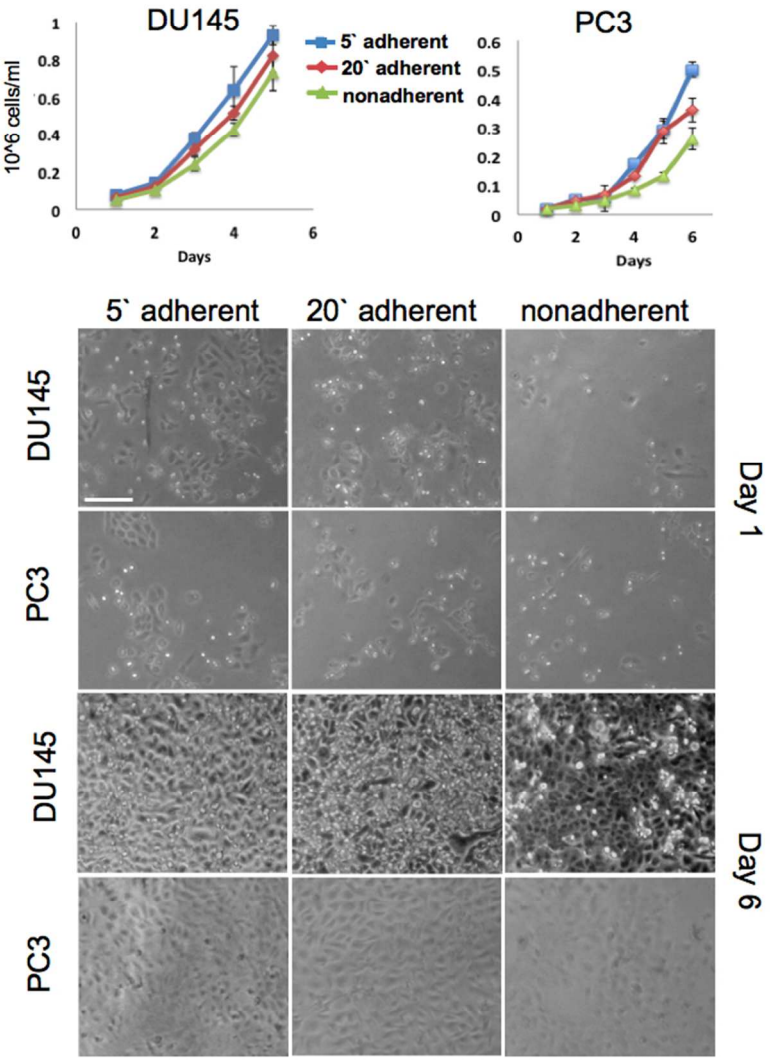
DU145
PC3
5` adherent
20` adherent
nonadherent
10^6 cells/ml
Days
5` adherent
20` adherent
nonadherent
DU145
PC3
DU145
PC3
Day 1
Day 6

FigS1

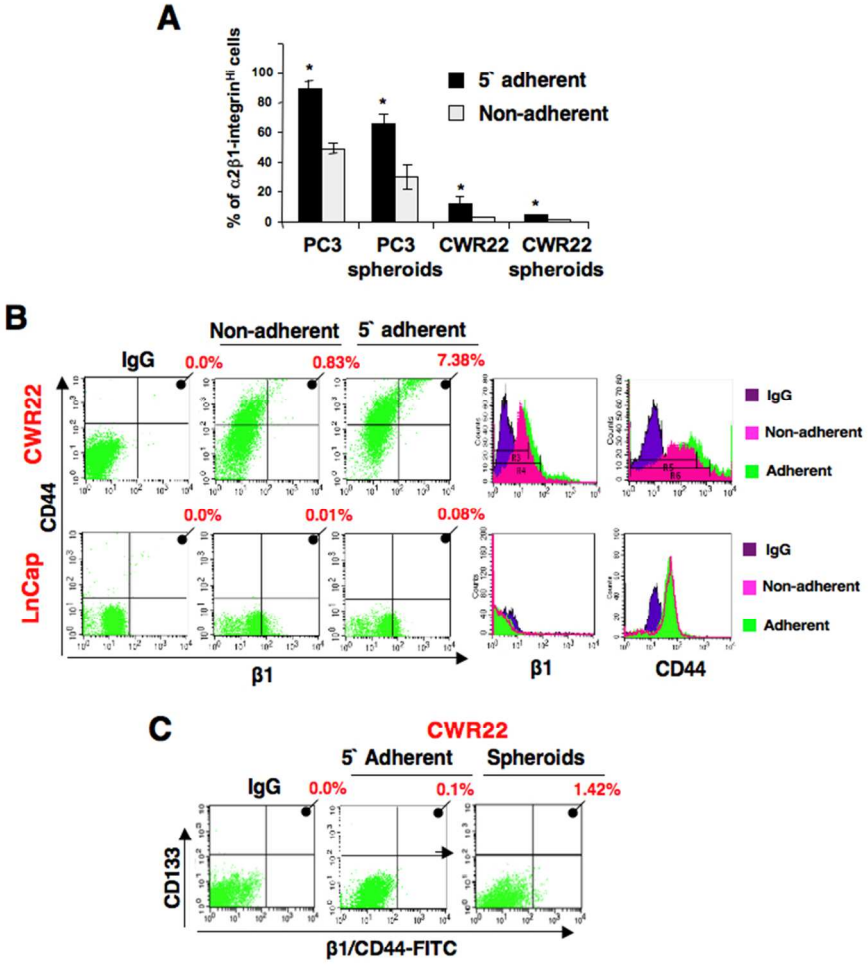
A
% of α2β1-integrin^Hi cells
100
80
60
40
20
0
5` adherent
Non-adherent
PC3
PC3 spheroids
CWR22
CWR22 spheroids
B
Non-adherent
5` adherent
IgG
0.0%
0.83%
7.38%
CWR22
CD44
LnCap
0.0%
0.01%
0.08%
β1
IgG
Non-adherent
Adherent
β1
CD44
C
CWR22
5` Adherent
Spheroids
IgG
0.0%
0.1%
1.42%
CD133
β1/CD44-FITC

FigS2

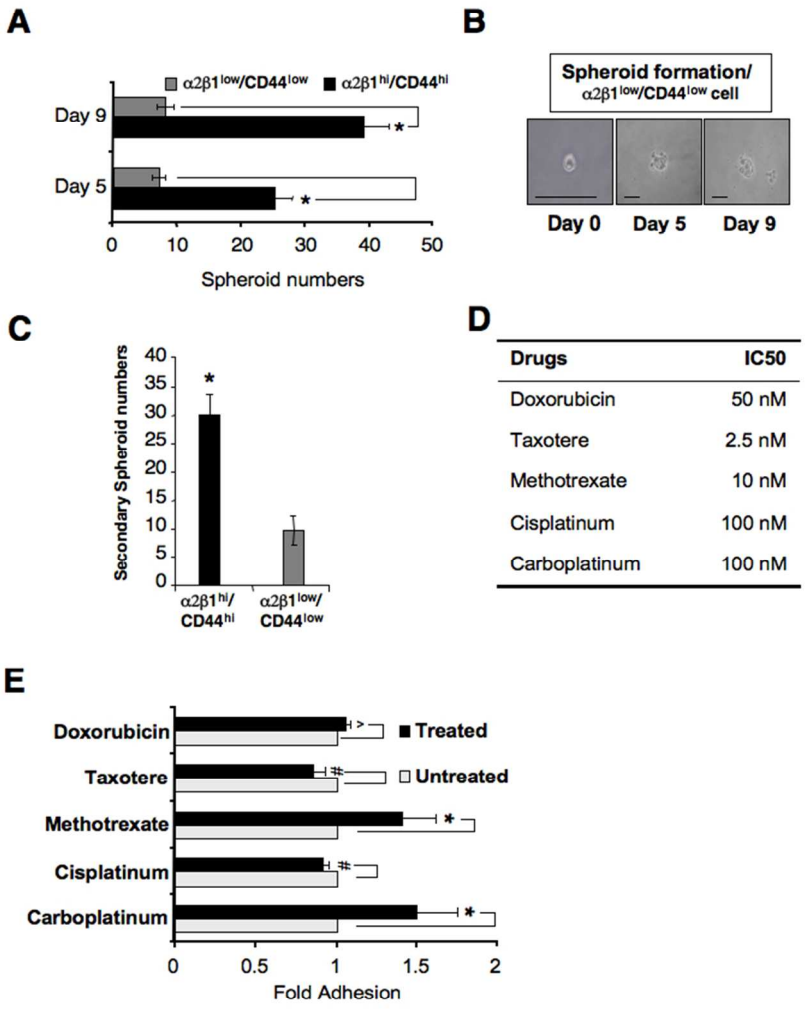
A
α2β1low/CD44low
α2β1hi/CD44hi
Day 9
Day 5
0 10 20 30 40 50
Spheroid numbers
B
Spheroid formation/
α2β1low/CD44low cell
Day 0
Day 5
Day 9
C
Secondary Spheroid numbers
0 5 10 15 20 25 30 35 40
α2β1hi/ CD44hi
α2β1low/ CD44low
D
Drugs IC50
Doxorubicin 50 nM
Taxotere 2.5 nM
Methotrexate 10 nM
Cisplatinum 100 nM
Carboplatinum 100 nM
E
Doxorubicin
Taxotere
Methotrexate
Cisplatinum
Carboplatinum
Treated
Untreated
0 0.5 1 1.5 2
Fold Adhesion

FigS3

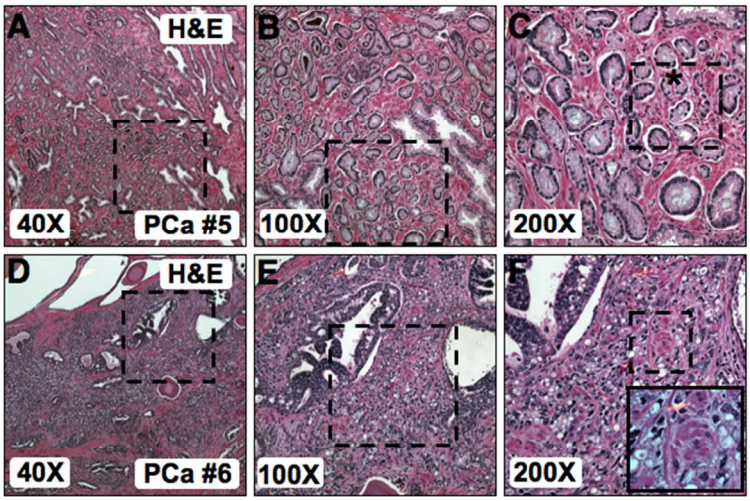

FigS4

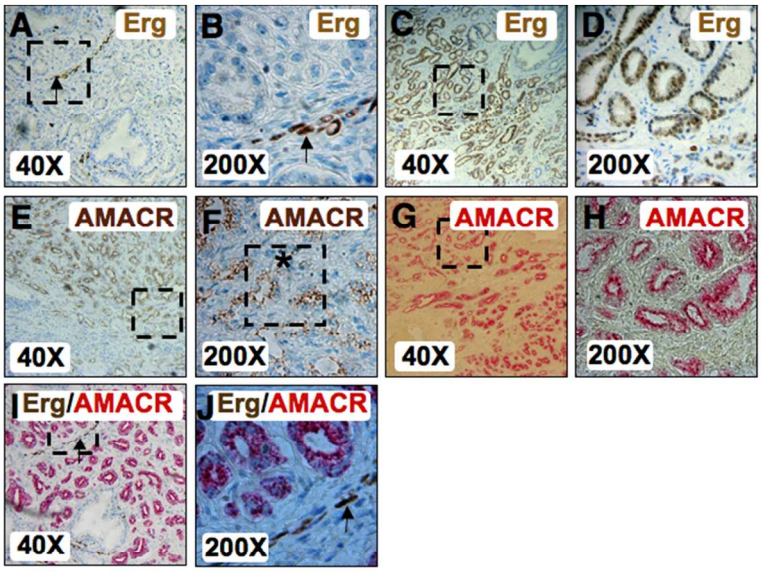
A
Erg
40X
B
Erg
200X
C
Erg
40X
D
Erg
200X
E
AMACR
40X
F
AMACR
200X
G
AMACR
40X
H
AMACR
200X
I
Erg/AMACR
40X
J
Erg/AMACR
200X

FigS5

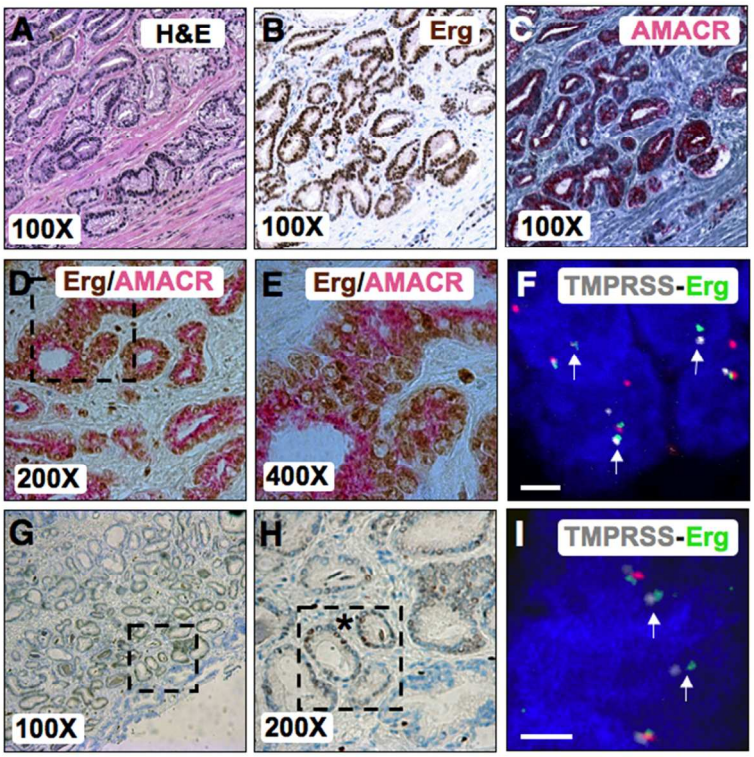
A
H&E
100X
B
Erg
100X
C
AMACR
100X
D
Erg/AMACR
200X
E
Erg/AMACR
400X
F
TMPRSS-Erg
G
100X
H
*
200X
I
TMPRSS-Erg

FigS6

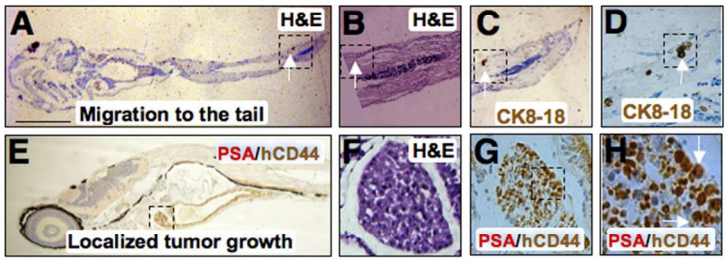
A
H&E
Migration to the tail
B
H&E
C
CK8-18
D
CK8-18
E
PSA/hCD44
Localized tumor growth
F
H&E
G
PSA/hCD44
H
PSA/hCD44

FigS7

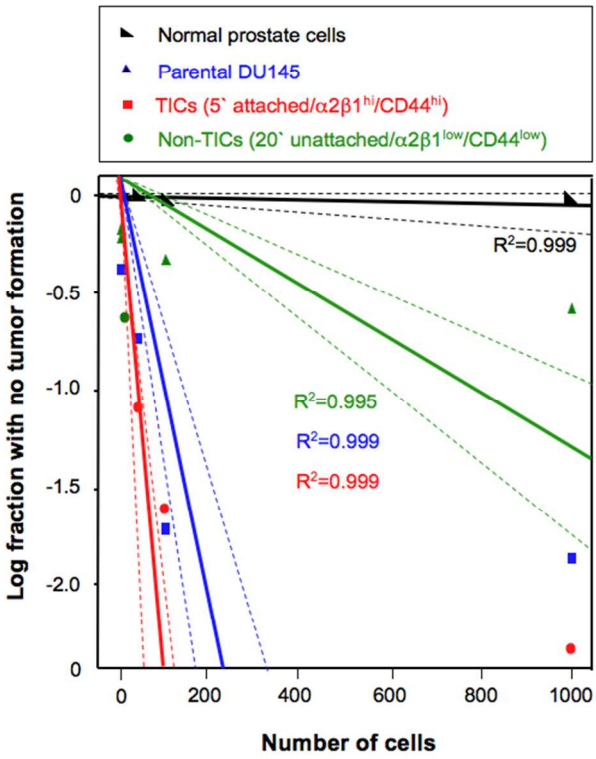
Normal prostate cells
Parental DU145
TICs (5` attached/α2β1hi/CD44hi)
Non-TICs (20` unattached/α2β1low/CD44low)
Log fraction with no tumor formation
0
-0.5
-1.0
-1.5
-2.0
0
R2=0.999
R2=0.995
R2=0.999
R2=0.999
0
200
400
600
800
1000
Number of cells

FigS8

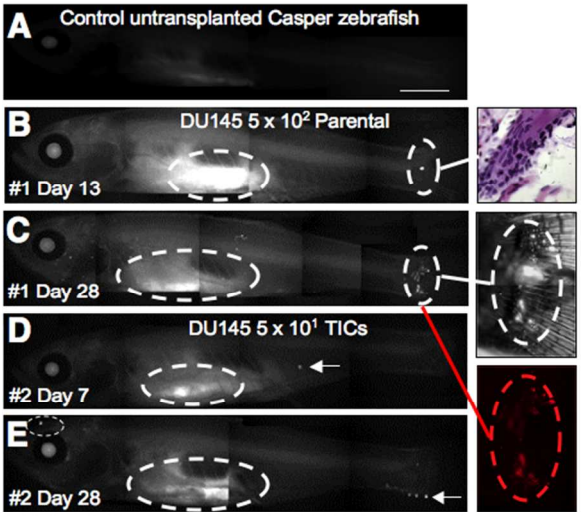
A
Control untransplanted Casper zebrafish
B
DU145 5 x 10² Parental
#1 Day 13
C
#1 Day 28
D
DU145 5 x 10¹ TICs
#2 Day 7
E
#2 Day 28

FigS9

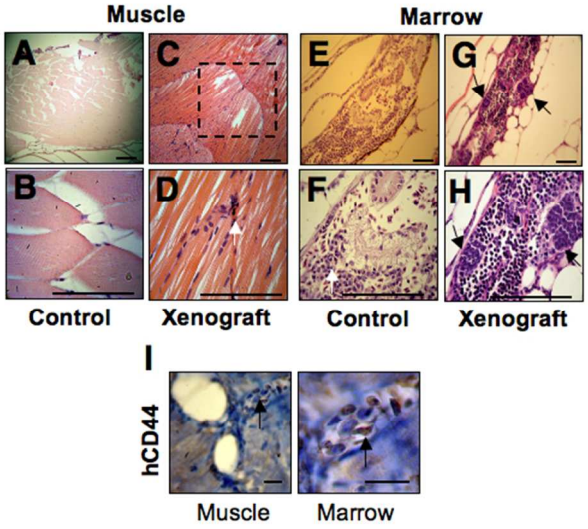
Muscle
Marrow
A
C
E
G
B
D
F
H
Control
Xenograft
Control
Xenograft
I
hCD44
Muscle
Marrow

FigS10